OLD DOMINION UNIVERSITY RESEARCH FOUNDATION

DEPARTMENT OF PHYSICS
COLLEGE OF SCIENCES
OLD DOMINION UNIVERSITY
NORFOLK, VIRGINIA 23508

TECHNICAL REPORT PTR-86-6

SUPPORT OF VALIDATION OF SAGE II DATA

Gary E. Copeland, Principal Investigator

Final Report
For the period ending December 31, 1986

Prepared for the
National Aeronautics and Space Administration
Langley Research Center
Hampton, Virginia 23665

Under
Cooperative Agreement NCC1-96
Mr. Leonard R. McMaster
ASD-Aerosal Research Branch

November 1986

DEPARTMENT OF PHYSICS
COLLEGE OF SCIENCES
OLD DOMINION UNIVERSITY
NORFOLK, VIRGINIA 23508

TECHNICAL REPORT PTR-86-6

SUPPORT OF VALIDATION OF SAGE II DATA

Gary E. Copeland, Principal Investigator

Final Report
For the period ending December 31, 1986

Prepared for the
National Aeronautics and Space Administration
Langley Research Center
Hampton, Virginia 23665

Under
Cooperative Agreement NCC1-96
Mr. Leonard R. McMaster
ASD-Aerosal Research Branch

Submitted by the
Old Dominion University Research Foundation
P.O. Box 6369
Norfolk, Virginia 23508

November 1986

SUPPORT OF VALIDATION OF SAGE II DATA

By

Gary E. Copeland[1] and O. Uchino[2]

SUMMARY

The enclosed articles describe the project work performed under NASA Cooperative Agreement NCC1-96, and are submitted in fulfillment of the final report requirement.

[1] Professor, Department of Physics, Old Dominion University, Norfolk, Virginia 23508.
[2] Research Associate, Department of Physics, Old Dominion University, Norfolk, Virginia 23508.

Submitted to Applied Optics
March, 1985

On temperature retrievals by Rayleigh backscatter lidar signals

O. Uchino*, M. P. McCormick° and T. J. Swissler+

* Old Dominion University Research Foundation
P.O. Box 6369, Norfolk, VA 23508

° Atmospheric Sciences Division
NASA Langley Research Center, Hampton, VA 23665

+ SASC Technologies Inc., Hampton, VA 23666

---

* Visiting Research Scientist from
Meteorological Research Institute, Tsukuba,
Ibaraki 305, Japan

Atmospheric temperature profiles can be deduced from the molecular density profiles assuming hydrostatic equilibrium for the atmosphere where the density profiles can be obtained from the Rayleigh backscatter lidar signal profiles. Hauchecorne and Chanin[1] have used this technique to measure temperature above 35 km altitude where aerosol scattering is considered negligible compared with Rayleigh backscattering. The lowest altitude at which temperature can be retrieved using a single wavelength lidar extends to about 30 km, depending on the upper boundary of the stratospheric aerosol layer.

For the case of background aerosols, Russell and Morley[2] proposed retrieving temperature in the lower stratosphere using two wavelength lidar signals. The technique consists of retrieving the aerosol backscatter profile at the long wavelength, then modeling a wavelength conversion factor for the aerosol backscatter at the short wavelength (approximately 0.35 μm). The estimated aerosol backscatter profile is combined with the measured signal at the short wavelength to yield molecular density profile which is used to retrieve temperature. Error analyses of temperature retrievals from spaceborne lidar have previously made.[2,3]

In this letter, differences between retrieved temperature T from lidar and atmospheric model temperature T_s are calculated for the following problems which except for problem b below have not been simulated so far.

a. Effect of a transient thin aerosol layer at any altitude on temperature retrieved by a single wavelength lidar.

b. Effect of residual aerosols which are not perfectly corrected for using a modeled wavelength conversion factor on temperature retrieved by a two wavelength lidar.

c. Errors due to splicing two backscatter signals which are obtained seperately.

d. Effect of multiple scattering.

Fig.1 shows lidar signals normalized to the Rayleigh backscatter signal expected from a model atmosphere[4] for the above four cases. To calculate the temperature difference $\Delta T=T-T_s$, lidar parameters used for the LITE (Lidar In-Space Technology Experiment) simulations[3] have been used. However, results denoted below can be applied to other lidar parameters if sufficient backscatter signals are obtained.

Fig.2 presents vertical profiles of the temperature difference ΔT simulated for above four cases. The small temperature difference at about 50 km is due to the boundary condition of temperature, T_s + 40 K, assumed at 90 km. The results shown in Fig.2 are summarized as follows:

a. At 34 km a ΔT of -8.3 K occurs due to the transient aerosol layer of scattering ratio 1.04. At 33 km it is about 1.2 K and approaches zero at 20 km. It is easy to distinguish a transient thin aerosol layer or noise with 4 percent excess signal above expected from Rayleigh backscatter from retrieved temperature profile.

b. Effects of an unknown residual aerosol backscatter of $\leq$ 1.2 % affect the retrieved temperature by $\leq$ -1.25 K. As the maximum scattering ratio at a wavelength of 355 nm is about 1.04 (4 percent aerosol contribution) for background stratospheric aerosols,

c. A discontinuity of ΔT equal to -4.2 K occurs at 30 km for a 2 percent splicing error constant below 30 km. ΔT approaches to zero exponentially downwards. To keep this temperature discontinuity below 2 K, it is necessary to splice two lidar backscatter signals with about one percent accuracy.[5] LITE will utilize only one photomultiplier channel and thus will not use splicing in its data analysis.

d. Effects of multiple scattering is assumed to be 4.4 percent at 4 km and to decrease upwards in proportion to atmospheric densities.[6] The calculated temperature difference is - 5 K at 4 km and approaches zero exponentially upwards. It is about - 1 K at 15 km. If lidar parameters such as receiver field of view and lidar system altitude are known, the effects of multiple scattering can be corrected to some extent theoretically.[6]

From these simulations, it is evident that temperature can be retrieved for $\pm$ 3 K, if Rayleigh backscatter can be measured for $\pm$ 1.5 percent. This is not unreasonable for a carefully developed lidar system. The LITE lidar in a 240 km orbit aboard shuttle should be able to make $\pm$ 3 K measurements from about 10-40 km, with vertical resolutions of 1 km and horizontal resolutions of 300 km.

One of us (O. Uchino) is supported by NASA Grant No. NCC1-96.

References

1. A. Hauchecorne and M. L. Chanin, " Density and Temperature Profiles Obtained by Lidar between 35 km and 75 km," Geophys. Res. Lett., 7, 565(1980).
2. P. B. Russell and B. M. Morley, " Orbiting Lidar Simulations. 2: Density, Temperature, Aerosol, and Cloud Measurements by a Wavelength-Combining Technique," Appl. Opt., 21, 1554(1982).
3. M. P. McCormick and T. J. Swissler, Private Communication (1985).
4. U. S. Standard Atmosphere (U. S. GPO, Washington, D. C., 1976).
5. P. B. Russell, B. M. Morley, J. M. Livingston, G. W. Grams, and E. M. Patterson, " Orbiting Lidar Simulations. 1: Aerosol and Cloud Measurements by an Independent-Wavelength Technique," Appl. Opt., 21, 1541(1982).
6. J. D. Spinhire, " Lidar Clear Atmosphere Multiple Scattering Dependence on Receiver Range," Appl. Opt., 21, 2467(1982).

Figure Captions.

Fig. 1. Excess lidar signals normalized to Rayleigh backscatter signals for four cases : a. transient thin aerosol layer, b. residual aerosols, c. splicing error, and d. multiple scattering.

Fig. 2. Temperature difference between temperature T retrieved by lidar and model temperature T_s for four cases in Fig.1.

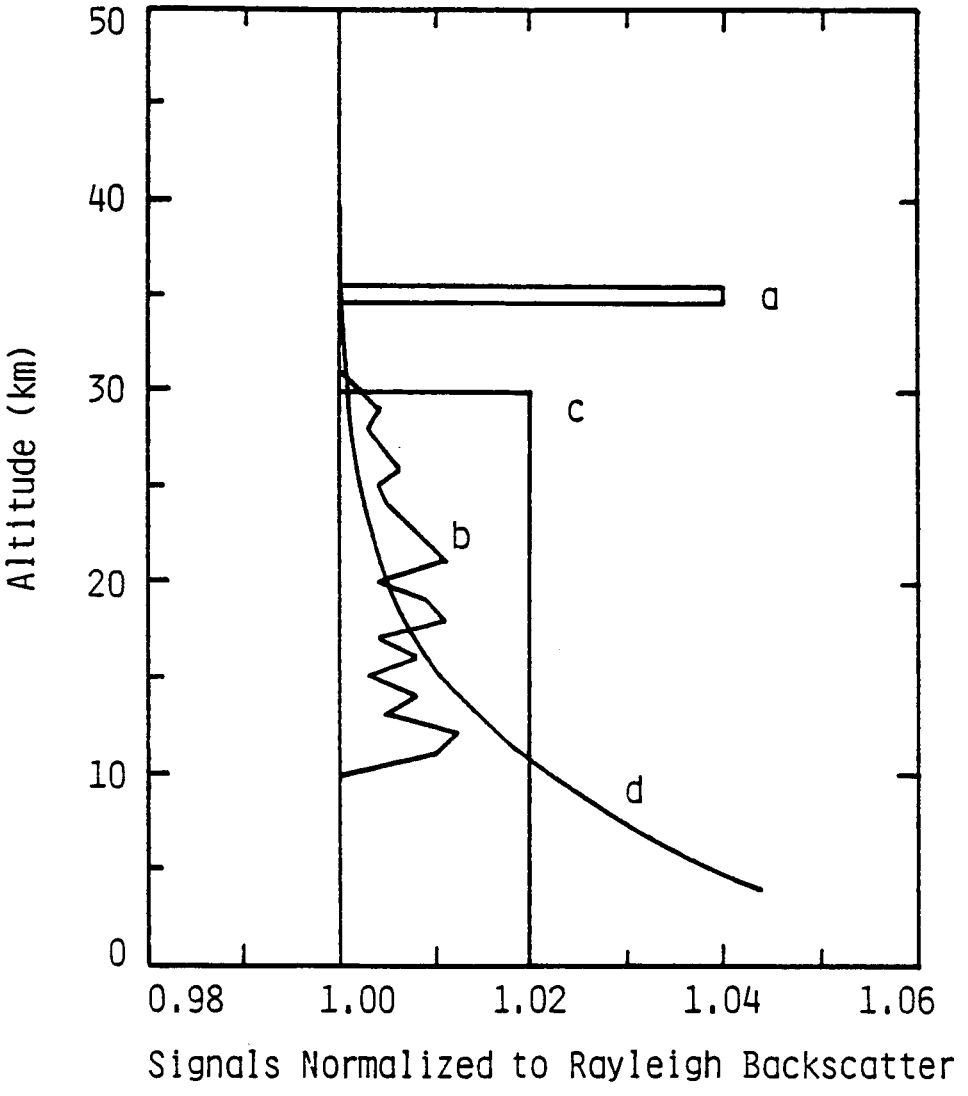
50
40
30
20
10
0
Altitude (km)
a
b
c
d
0.98
1.00
1.02
1.04
1.06
Signals Normalized to Rayleigh Backscatter

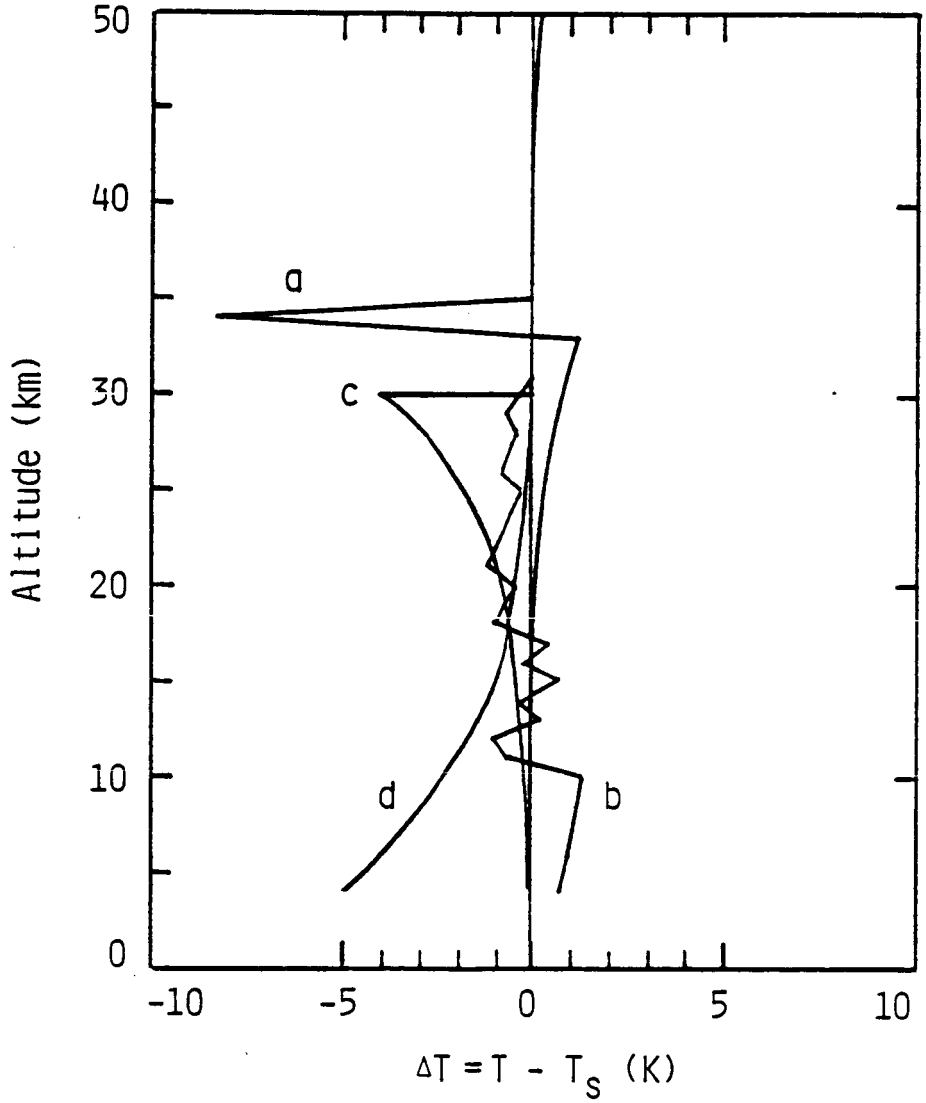
50
40
30
20
10
0
Altitude (km)
a
c
d
b
-10
-5
0
5
10
ΔT = T - T_S (K)

Submitted to Applied Optics
M.S.A. -86

Error Analysis of DIAL Measurements of Ozone by a Shuttle Excimer Lidar

O. Uchino*, M. P. McCormick°, T. J. Swissler+ and L. R. McMaster°

* Old Dominion University Research Foundation
P.O. Box 6369, Norfolk, VA 23508

° Atmospheric Sciences Division
NASA Langley Research Center, Hampton, VA 23665

+ SASC Technologies Inc., Hampton, VA 23666

* Visiting Research Scientist from
Meteorological Research Institute, Tsukuba,
Ibaraki 305, Japan

Abstract

An error analysis of DIAL (Differential Absorption Lidar) measurements of stratospheric ozone from a Space Shuttle is discussed. A transmitter system consisting of a KrF excimer laser pumping gas cells of H_2 or D_2 producing output wavelengths in the near uv is shown to be useful for the measurement of ozone in an altitude range from 15-50 km.

I. Introduction

Measurements of ozone in the lower stratosphere have been conducted using a lidar incorporating an XeCl laser with supporting meteorological data.[1,2] Differential absorption lidar (DIAL) measurements of ozone in the lower stratosphere have been conducted using frequency-doubled dyes pumped by a Nd:YAG laser.[3] DIAL measurments of ozone in the middle and upper stratosphere above 25 km altitude have been made using an XeCl laser pumping a cell of methane gas producing the first Stokes line of methane.[4] In addition, DIAL measurements of ozone above 25 km have been conducted using the third harmonic of a Nd:YAG laser plus the fundamental output of an XeCl laser.[5]

As above, DIAL measurements of ozone appear feasible up to an altitude of 50 km by a ground-based XeCl laser. However, it takes several hours to measure ozone densities at 40-45 km even if an efficient XeCl laser is used with an output energy of 250 mJ per pulse and a repetition rate of 50 Hz.[5] This is due to the strong absorption of ozone below 40 km. In the DIAL measurements of ozone from a shuttle, this strong absorption can be avoided and global data can be obtained in a short time with high accuracies as denoted below. The global data will be useful in the analysis of ozone transport in the stratosphere and for studying long term trends in ozone.

This paper will calculate the errors associated with and, therefore, explore the feasibility of the measurement of stratospheric ozone from a spaceborne instrument aboard shuttle.

II. Methodology of Error Analysis

The mean ozone concentration $\bar{n}(z)$ within an altitude interval of z and $z'=z + \Delta z$ can be obtained by the DIAL measurement as given in the following:

$$\bar{n}(z)= \frac{1}{2\ \Delta\sigma\ \Delta z} \ln \left[\frac{P_1(z)}{P_1(z')} \Big/ \frac{P_2(z)}{P_2(z')} \right] + B + E \qquad (1)$$

where

$$B = \frac{1}{2\ \Delta\sigma\ \Delta z} \ln \left[\frac{\beta_1(z')}{\beta_1(z)} \Big/ \frac{\beta_2(z')}{\beta_2(z)} \right], \qquad (2)$$

$$E = \frac{1}{\Delta\sigma\ \Delta z} \int_z^{z'} (\alpha_{R1} - \alpha_{R2} + \alpha_{M1} - \alpha_{M2}) dz$$

$$= \frac{1}{\Delta\sigma} (\bar{\alpha}_{R1} - \bar{\alpha}_{R2} + \bar{\alpha}_{M1} - \bar{\alpha}_{M2}) \qquad (3)$$

and $P_i(z)$ (i=1,2) is the total received number of photoelectrons from an altitude z with a small range δz, and $\Delta\sigma$ is the differential ozone absorption cross section ($\Delta\sigma=\sigma_2 - \sigma_1$). $\beta_i(z)$ is the atmospheric backscattering coefficient at wavelength i and altitude z. α_R and α_M are Rayleigh and Mie extinction coefficients, respectively.

In general the DIAL measurement of $\bar{n}(z)$ is made using the first term in Eq. (1). For this approximation, the relative uncertainty $\varepsilon = \Delta\bar{n}/\bar{n}$ can be expressed by[6]

$$\varepsilon^2 = \varepsilon_1^2 + \varepsilon_2^2 \tag{4}$$

where

$$\varepsilon_1 = \frac{1}{2\,\Delta\sigma\,\bar{n}\,\Delta z}\left\{\sum_{i=1}^{2}\left(\frac{P_i(z) + 2P_b}{P_i^2(z)} + \frac{P_i(z') + 2P_b}{P_i^2(z')}\right)\right\}^{1/2} \tag{5}$$

$$\varepsilon_2 = (B + E)/\bar{n}$$

P_b is background noise, ε_1 denotes a statistical error due to the signal and background fluctuations, and ε_2 is a systematic error due to the assumption of B=E=0.[3,7] As the two wavelengths can be emitted simultaneously, the errors due to temporal variations of B and E are not taken into account.

III. Lidar System Parameters

Figure 1 depicts the transmitter system for the proposed DIAL system. A KrF laser pumping gas cell of either H_2 or D_2 produces four wavelengths; the fundamental of KrF plus three Stokes lines of H_2 or D_2.[8,9] The output energy of the KrF laser is 300 mJ with a pulse width of 10-20 ns and a pulse repetition frequency of 100 Hz. The energy conversion efficiencies of these Stokes lines S_1, S_2, and S_3 are assumed to be 20, 20, and 10 percent, respectively.[10-12] In these simulations, ozone absorption cross sections from Inn and Tanaka[13], the U.S. Standard Atmosphere[14], and a mid-latitude ozone profile[15] are used, and the aerosol models employed are taken from Shettle and Fenn.[16]

IV. Simulation

The total number of signal photoelectrons $P_i(z)$, for a vertical range of 1 km (δz=1 km) and the output energies shown in Table I, are shown in Fig. 2. The total shot number of laser pulses is 10,000 shots. From the figure, it is clear that photoelectron counters should be used for the detection system. A fast speed counter and photomultiplier tube (PMT) with fast rise time having a counting linearity up to about 50 photoelectrons per shot for a time gate interval of 6.66 μs (δz=1 km)[17] is required.

Figure 3 shows the error analysis for the wavelength pairs consisting of the KrF laser and H_2 cell. The horizontal resolution is 800 km (10^4 shots at 100 Hz). The vertical resolution is 1 km ($\delta z=\Delta z$=1 km) below 50 km altitude and 2 km ($\delta z=\Delta z$=2 km) above it. The solid lines in the figure show the relative uncertainties for a moonless nighttime when the total number of photoelectrons due to background noise is below 5 in the wavelength range of 248-360 nm.[18] The dashed lines show the uncertainties for a case of higher noise-occurrence-probabilities of 0.1 background photoelectron per shot for a wavelength region of 248 - 313 nm, 0.2 background photoelectron per shot for ≈320nm, and 0.5 background photoelectrons per shot for ≈360 nm. The kinks in the line around 50 km in the figure are due to the difference of vertical resolution above and below 50 km.

For the wavelength pairs of 248.4 - 313.0 nm and 277.0 - 313.0 nm, the relative uncertainties of ozone densities measured by the DIAL technique are within 10 percent for 37 - 48 km altitude for a moonless nighttime. In this altitude range, the errors due to neglecting B and E are less than 0.3 percent. If the output energies at these wavelengths are increased by a factor of 2, the relative uncertainties are decreased by a factor of $\sqrt{2}$. These wavelength pairs are most useful for ozone measurements in the region of 40-45 km where the effect of CFM's on the long term ozone concentration is considered to be large.

The wavelength pair of 313.0 - 359.8 nm is available for ozone measurements in the lower altitude range of 12 - 27 km. In this case, the errors in $\bar{n}(z)$ due to neglecting the term $\bar{\alpha}_{R1} - \bar{\alpha}_{R2}$ in Eq. (3) are large below 18 km altitude. The dotted line in Fig. 3 shows the relative uncertainties of ozone densities calculated by using E' instead of E in Eq. (6) where $E'=(0.25 \times (\bar{\alpha}_{R1}-\bar{\alpha}_{R2}) + (\bar{\alpha}_{M1} - \bar{\alpha}_{M2}))/\Delta\sigma$, and n is estimated by the first term in Eq. (1) plus $(\bar{\alpha}_{R1}- \bar{\alpha}_{R2})/\Delta\sigma$. The factor 0.25 corresponds to a standard deviation of atmospheric density.[14]

The relative uncertainties of the DIAL measurement of ozone increase in the altitude range 27 - 34 km. This can be overcome by using a gas cell of D_2 instead of H_2. Figure 4 shows the relative uncertainties of the DIAL measurement of ozone using the stimulated Raman scattering lines of D_2. The solid lines in the figure show the relative uncertainties for a moonless night, and the dashed lines show them for a case of higher noise-occurrence-probabilities as mentioned above. As can be seen, the wavelength pair 291.8 - 319.6 nm is useful for the DIAL measurement of ozone in an altitude range of 25 - 40 km. Figures 3 and 4 show that if gas cells of H_2 and D_2 are pumped simultaneously by a high powered KrF laser, accurate DIAL measurements of ozone are possible in an altitude range of 15 - 50 km using these combinations of wavelengths.

A. Effect of Aerosol

Stratospheric aerosols will have an effect on DIAL ozone retrievals at the altitudes where they reside, approximately from the tropopause to 10 km above the tropopause. The magnitude of their effect will depend of course on the amount present in the stratosphere which is dependent on volcanic perturbations. Effects of the aerosol model assumed in the simulations on the total

errors for the wavelength pair of 313.0 - 359.8 nm have been analyzed. Figure 5 shows three aerosol models for 313.0 nm: background, aged volcanic, and fresh volcanic.[16] The results of the uncertainties in ozone density for these models are shown in Fig. 6, where E' is also used to calculate ε_2. For the fresh volcanic aerosol model (dashed line), the relative uncertainty is large. The minimum of the uncertainty around 19 km is due to an assumption that the aerosols are constant vertically in spite of the maximum of the content. In this case, the following procedure might decrease the uncertainty. The aerosol distribution is first obtained from the wavelength of 359.8 nm. Then the effects of aerosols on the 313.0 nm wavelength are extrapolated from 359.8 nm. These cases are also encountered in the DIAL measurement of ozone in the boundary layer.[19] Unfortunately, both fresh volcanic aerosols and boundary layer aerosols are difficult to model. Another method to decrease the errors is to use an appropriate wavelength pair with a small difference of wavelength.[3]

B. Effect of temperature

The ozone absorption cross sections are temperature dependent. Figure 7 shows the relative variations of the absorption cross sections at seven wavelengths in a temperature range 214-291 K.[20] These wavelengths are near the laser wavelengths used for the DIAL simulations. In the wavelengths shorter than 291.4 nm, the relative temperature variations of the cross sections are several percent, but they are 20-30 percent in the wavelengths longer than 300 nm. For the cross section variations, an additional term ε_3^2 is included in Eq. (4), where

$$\varepsilon_3^2 = \left(\frac{\Delta\sigma}{\sigma}\right)^2 = \left(\frac{\Delta\sigma_1}{\sigma}\right)^2 \left(\frac{\Delta\sigma_1}{\sigma_1}\right)^2 + \left(\frac{\Delta\sigma_2}{\sigma}\right)^2 \left(\frac{\Delta\sigma_2}{\sigma_2}\right)^2 \qquad (7)$$

For the wavelength pairs used for the simulations so far, it was approximated that $\sigma_1/\sigma \approx 1$ and $\sigma_2/\sigma \leq 0.1$. Therefore, in spite of the large temperature variations of σ_2, ε_3^2 is roughly equal to or smaller than $2(\Delta\sigma_1/\sigma_1)^2$. To obtain the ozone density with a high accuracy, therefore, it will be necessary to measure temperature with an accuracy of 5-10 K.

Figure 8 shows the U.S. Standard Atmosphere model of temperature, T_s. The arrows in the figure show the lowest and highest mean monthly temperatures obtained for any location between the Equator and pole.[14] Atmospheric temperatures will change greatly during a shuttle orbit covering both hemispheres. Temperature retrievals from the non-DIAL or backscatter lidar measurements at 359.8 nm are obtained by using the perfect gas law and hydrostatic equilibrium.[21] The U.S. atmosphere model is also used for the simulation. The effect of aerosols is neglected above 30 km. As a boundary condition of temperature, two cases of T_s+40 K (solid line (1) to right of center line) and T_s - 60 K (solid line (2) to left) at 90 km are assumed. As shown in the figure, deviations from the model (center line) are very small below 65 km altitude for the two boundary conditions. At 60 km, for example, this difference is less than 0.7K. Temperature retrievals below 60 km, therefore, do not depend on the boundary conditions.[21] These measurements are accomplished with only one wavelength.

Figure 9 shows the accuracy in temperature measurements for various output energies per pulse using the above one wavelength technique. The boundary condition of temperature at 90 km is assumed to be T_s+40 K. The vertical resolutions are 1 km ($\delta z=\Delta z=1$ km) below 50 km altitude and 2 km ($\delta z=\Delta z=2$ km) above it. As the output energy of the laser increases, measurement errors of temperature decrease. Even for low output energies, it appears possible to measure vertical distributions of temperature with an accuracy of 2-5 K in the region of 40 km altitude. Simulations of temperature retrievals for LITE (Lidar In-Space Technology Experiment), for example, using the tripled wavelength of a Nd:YAG laser (355 nm) shows similar results in that temperatures can be retrieved to ±3K between 15 and 30 km during background aerosol conditions.[22]

V. Conclusion

A shuttle lidar system based on a KrF excimer laser pumping a Raman cell of H_2 or D_2 producing the fundamental wavelength and the Stokes lines of H_2 and D_2 are shown to provide an accuracy useful for the DIAL measurement of ozone in the middle and upper stratosphere. The relative uncertainties of ozone densities measured at night by this DIAL system are within 10 percent in the altitude range 30-47 km with a vertical resolution of 1 km and a horizontal resolution of 800 km. For a case of vertical resolution of 3 km ($\Delta z=3$ km, $\delta z=1$ km) with the same horizontal resolution, the relative uncertainties of ozone densities will be reduced to 2-3 percent. The errors due to temperature dependence of the absorption cross section of ozone will be smaller than 1 percent since atmospheric temperature can be measured within 10 K using a wavelength of 359.8 nm. DIAL measurements of ozone in the lower stratosphere using this shuttle lidar system depend on aerosol loading and our understanding of aerosols. For the increased levels of stratospheric aerosols experienced after violent volcanic eruptions, the relative uncertainties of ozone densities will be large in the region below about 24 km. DIAL measurements of ozone with good accuracy will be

useful for increasing our understanding of ozone in the middle and upper stratosphere.

One of us (O. Uchino) is supported by NASA Grant No. NCC1-96.

References

1. O. Uchino, M. Maeda, J. Kohno, T. Shibata, C. Nagasawa, and M. Hirono, "Observation of Stratospheric Ozone Layer by a XeCl Laser Radar," Appl. Phys. Lett., 33, 807 (1978).
2. O. Uchino, M. Maeda, H. Yamamura, and M. Hirono, "Observation of Stratospheric Vertical Ozone Distribution by a XeCl Lidar," J. Geophys. Res., 88, 5273 (1983).
3. J. Pelon and G. Megie, "Ozone Monitoring in the Troposphere and Lower Stratosphere: Evaluation and Operation of a Ground-Based Lidar Station," J. Geophys. Res., 87, 4947 (1982).
4. J. Werner, K. W. Rothe, and H. Walther, "Monitoring of the Stratospheric Ozone Layer by Laser Radar," Appl. Phys., B 32, 113 (1983).
5. G. J. Megie, G. Ancellet, and J. Pelon, "Lidar Measurements of Ozone Vertical Profiles," Appl. Opt., 24, 3454 (1985).
6. P. B. Russell, T. J. Swissler, and M. P. McCormick, "Methodology for Error Analysis and Simulation of Lidar Aerosol Measurements," Appl. Opt., 18, 3783 (1979).
7. G. Megie and R. T. Menzies, "Complementarity of UV and IR Differential Absorption Lidar for Global Measurements of Atmospheric Species," Appl. Opt., 19, 1173 (1980).
8. O. Uchino, M. Maeda, and M. Hirono, "Applications of Excimer Lasers to Laser-Radar Observations of the Upper Atmosphere," IEEE J. Quantum Electron., QE-15, 1094, (1979).
9. E. V. Browell, Ed., "Shuttle Atmospheric Lidar Research Program - Final Report of Atmospheric Lidar Working Group," NASA Spec. Publ. 433 (1979).
10. T. R. Loree, R. C. Sze, D. L. Barker, and P. B. Scott, "New Lines in the UV: SRS of Excimer Laser Wavelength," IEEE J. Quantum Electron., QE-15, 337 (1979).

11. O. Uchino, M. Tokunaga, M. Maeda, and Y. Miyazoe, "Differential-Absorption-Lidar Measurement of Tropospheric Ozone with Excimer-Raman Hybrid Laser," Opt. Lett., 8, 347 (1983).

12. T. Shibata, K. Seki, T. Hayami, M. Kobuchi, and M. Maeda, "Observation of Atmospheric Ozone by a Differential Absorption Lidar Using Excimer Raman Lasers," (in Japanese), Rev. Laser Eng., 13, 276 (1985).

13. E. C. Inn and Y. Tanaka, "Absorption Coefficient of Ozone in the Ultraviolet and Visible Region," J. Opt. Soc. Am., 43, 870 (1953).

14. U. S. Standard Atmosphere (U.S. GPO, Washington, DC, 1976), 227 pp.

15. A. J. Kruger and R. A. Minzer, "A Mid-Latitude Ozone Model for the 1976 U. S. Standard Atmosphere," J. Geophys. Res., 81, 4477 (1976).

16. E. P. Shettle and R. W. Fenn, "Models of the Atmospheric Aerosols and Their Optical Properties," AGARD Conference Proceedings No. 183, Lyngby, Denmark, AGARD-CP-83, NTIS, AD4028-65.

17. O. Uchino, K. Takahashi, I. Tabata, I. Akita, Y. Okada, and K. Naito, "Ruby Lidar Observations of El Chichon Dust Clouds at Tsukuba (36.1°N) and Comparisons with UV Lidar Measurements at Fukuoka (33.6°N)", J. Meteor. Soc. Japan, 62, 679 (1984).

18. T. Aruga and T. Igarashi, "Vertical Distribution of Ozone: A New Method of Determination using Satellite Measurements," Appl. Opt., 15, 261 (1975).

19. E. B. Browell, S. Ismail, and S. Shipley, "Ultraviolet DIAL Measurments of O_3 Profiles in Region of Spatially Inhomogeneous Aerosols," Appl. Opt., 24, 2827 (1985).

20. E. Vigroux, "Contribution experimentale a l'absorption de l'ozone, Ann. Phys. Paris, 8, 709 (1953).

21. A. Hauchecorne and M. L. Chanin, "Density and Temperature Profiles Obtained by Lidar between 35 and 70 km," Geophys. Res. Lett., 7, 565 (1980).

22. M. P. McCormick and T. J. Swissler, Private Communication (1985).

Table I. Shuttle Lidar Parameters Assumed for DIAL Measurement of Ozone

Transmitter							
Wavelength (nm)	248.4	268.3	277.0	291.8	313.0	319.6	359.8
Ozone absorption cross section (m^2)	1.05E-21	8.32E-22	5.05E-22	1.06E-22	6.0E-24	2.6E-24	5.9E-27
Energy per pulse (mJ)	150	60	60	60	60	30	30
Pulse repetition rate (Hz)	100	100	100	100	100	100	100
Receiver							
Telescope diameter	1.25 m		Optical efficiency		0.125		
Field of view	1 mrad		Quantum efficiency of photomultiplier		0.2		
Bandwidth	1 nm						
Space Shuttle							
Altitude	300 km						
Speed of footprint	8 km/s						

Figure Captions

Fig. 1 Depiction of DIAL transmitter system. S_i = the ith Stokes line. H_2 is hydrogen, D_2 deuterium.

Fig. 2 Total number of signal photoelectrons calculated by using the lidar system in Table 1.

Fig. 3 Uncertainty of ozone density measured by DIAL system using for KrF laser fundamental and SRS of H_2.

Fig. 4 Uncertainty of ozone density measured by DIAL system using for KrF laser fundamental and SRS of D_2.

Fig. 5 Model extinction coefficients at a wavelength of 313.0 nm.

Fig. 6 Uncertainty of ozone density measured by DIAL for the three aerosol models in Fig. 5.

Fig. 7 Temperature variations of absorption cross sections at seven wavelengths relative to 291 K.[20]

Fig. 8 Temperature model and retrievals from backscatter measurements at 359.8 nm for two boundary conditions at 90 km: (1) T_s + 40 K, and (2) T_s - 60 K.

Fig. 9 Temperature accuracy measured at a wavelength of 359.8 nm for different laser output energies. Dotted line shows temperature accuracy for increasing quantum efficiency to 0.25 and the optical efficiency to 0.20 for a laser output energy of 0.4 joules.

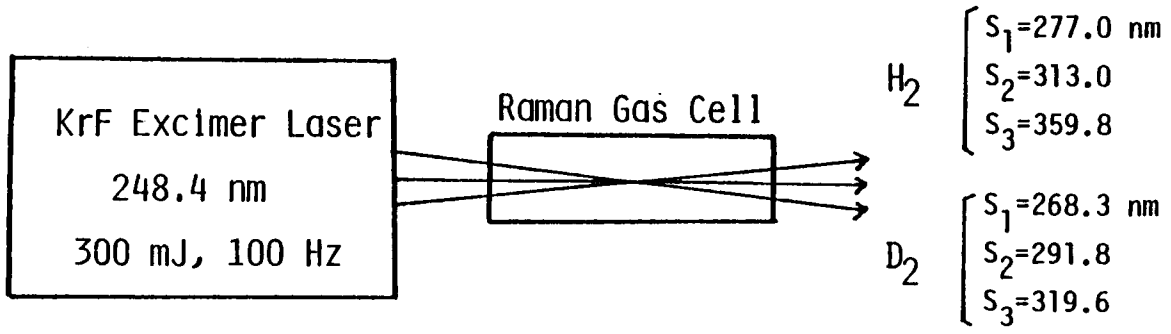
KrF Excimer Laser
248.4 nm
300 mJ, 100 Hz
Raman Gas Cell
H2
S1=277.0 nm
S2=313.0
S3=359.8
D2
S1=268.3 nm
S2=291.8
S3=319.6

Fig. 1

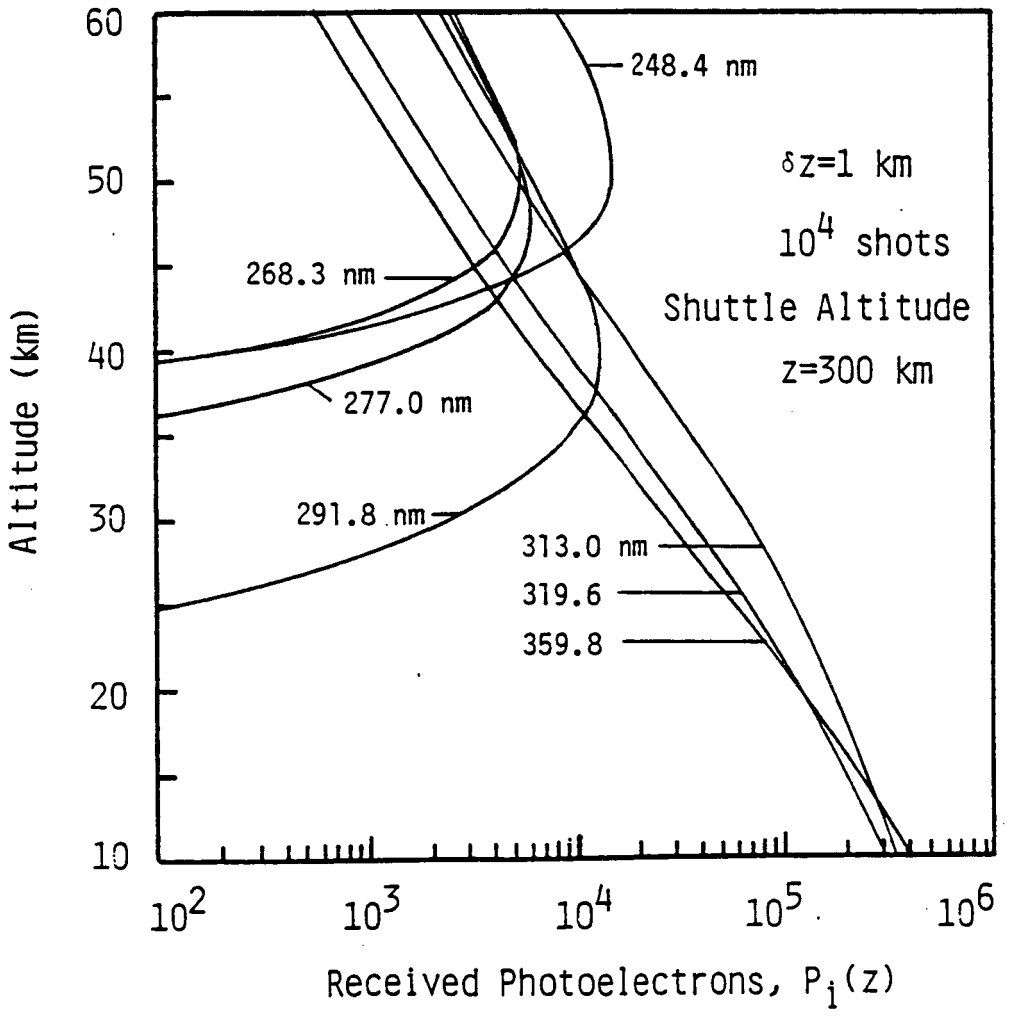
60
50
40
30
20
10
Altitude (km)
248.4 nm
δz=1 km
10^4 shots
Shuttle Altitude
z=300 km
268.3 nm
277.0 nm
291.8 nm
313.0 nm
319.6
359.8
10^2
10^3
10^4
10^5
10^6
Received Photoelectrons, P_i(z)

Fig. 2

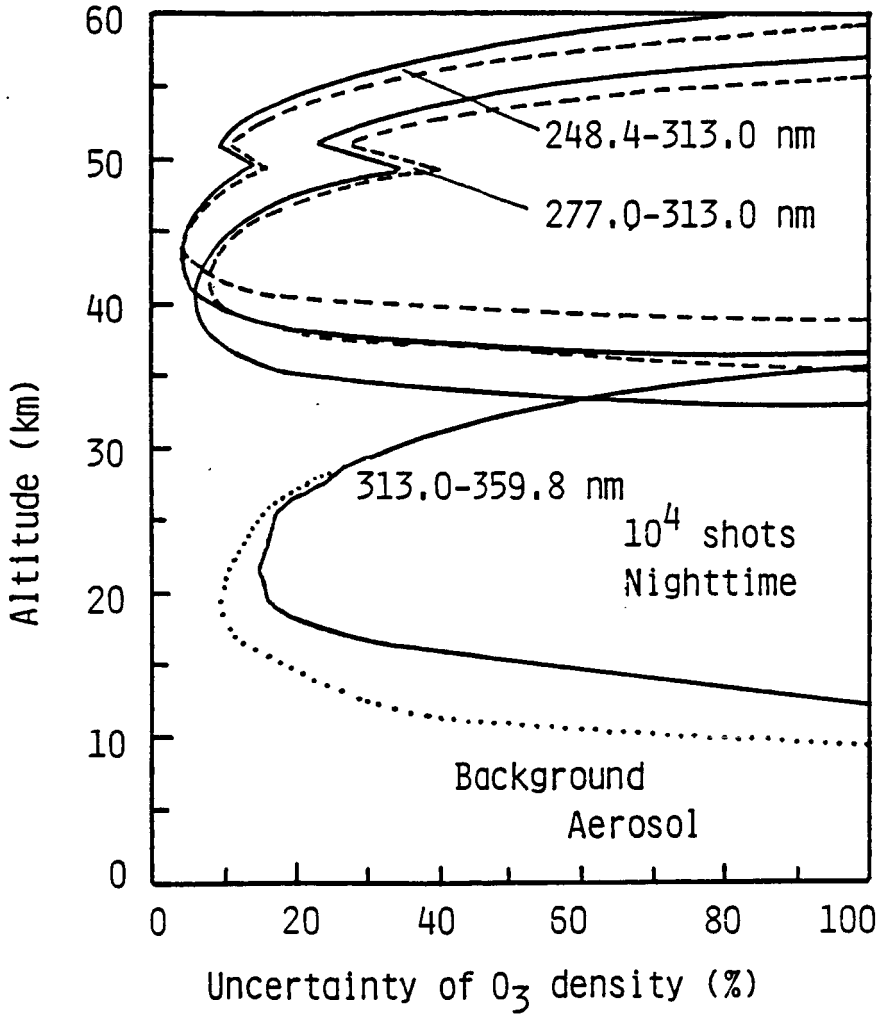
60
50
40
30
20
10
0
Altitude (km)
248.4-313.0 nm
277.0-313.0 nm
313.0-359.8 nm
10^4 shots
Nighttime
Background
Aerosol
0
20
40
60
80
100
Uncertainty of O_3 density (%)

Fig. 3

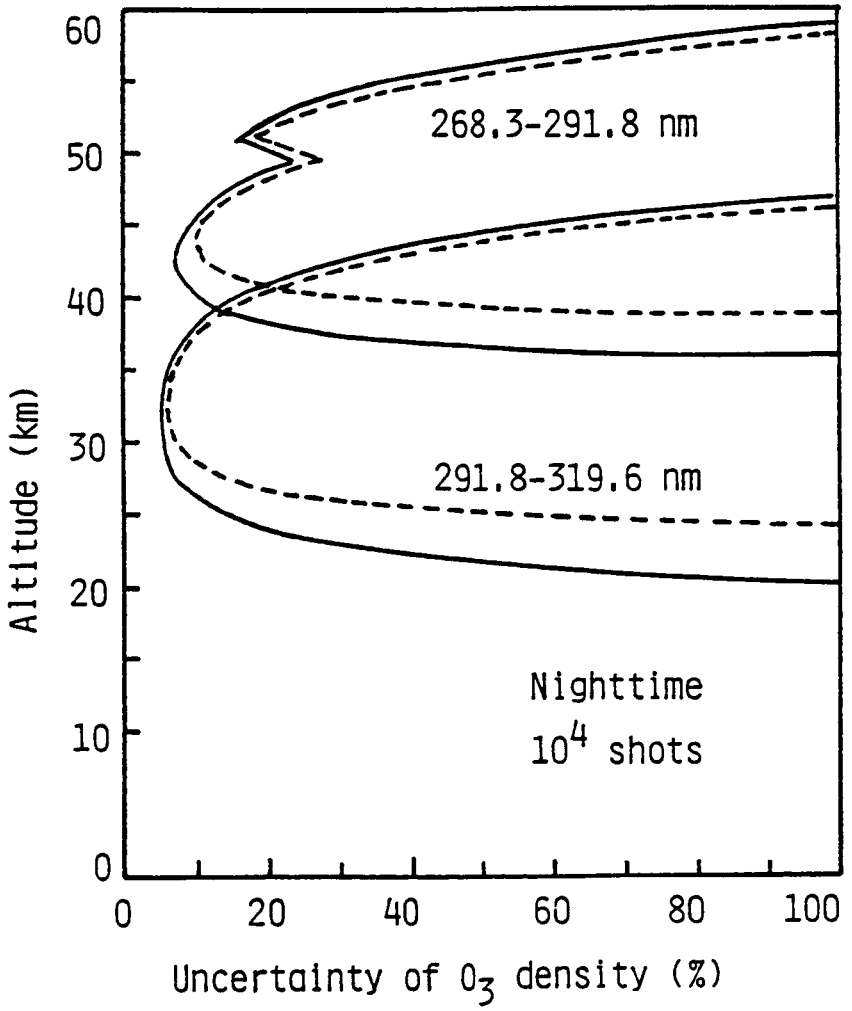
60
50
40
30
20
10
0
Altitude (km)
268.3-291.8 nm
291.8-319.6 nm
Nighttime
10^4 shots
0
20
40
60
80
100
Uncertainty of O_3 density (%)

Fig. 4

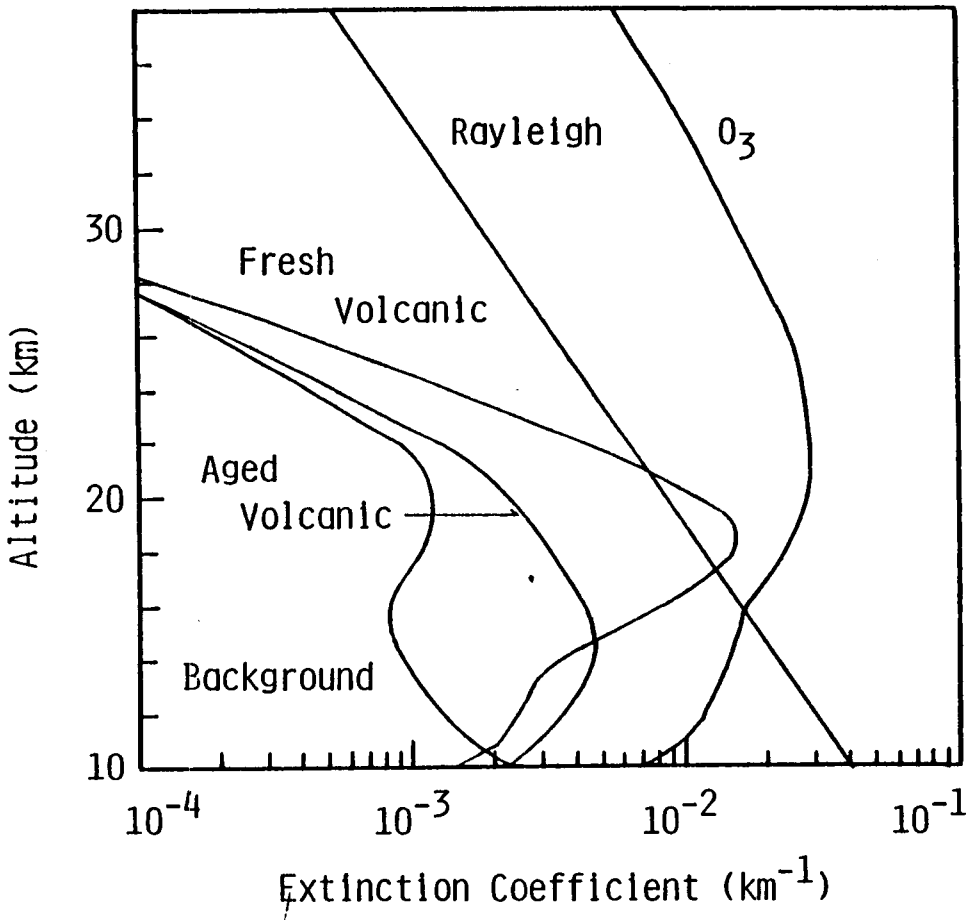
Rayleigh
O_3
Fresh
Volcanic
Aged
Volcanic
Background
30
20
10
Altitude (km)
10^{-4}
10^{-3}
10^{-2}
10^{-1}
Extinction Coefficient (km^{-1})

Fig. 5

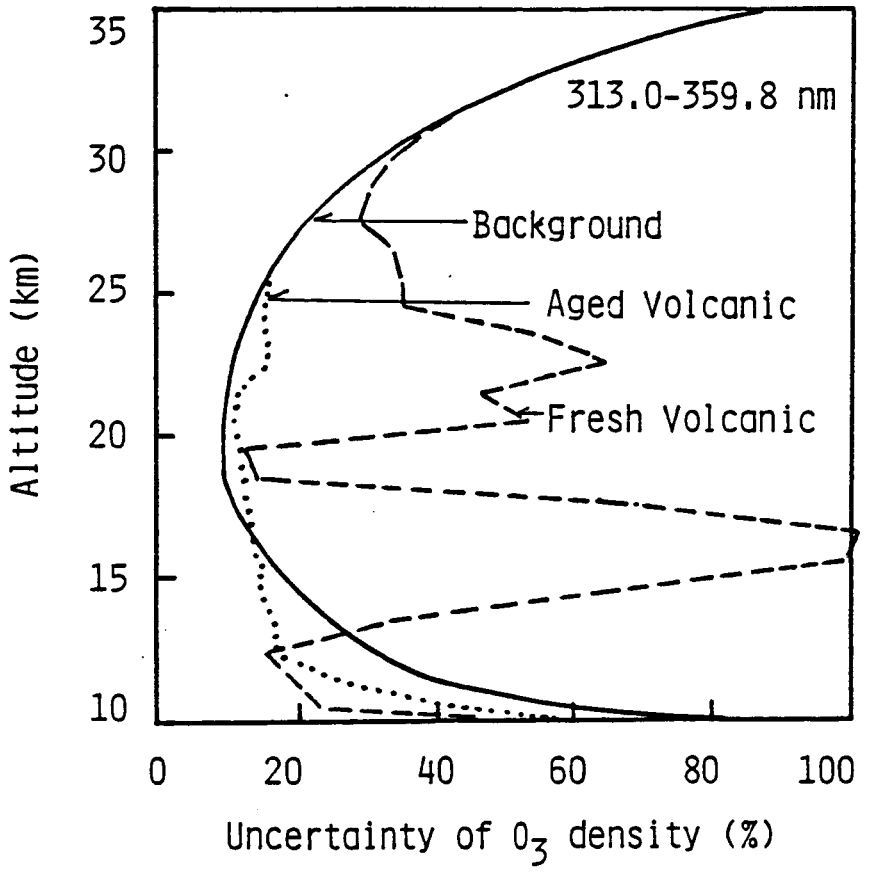
313.0-359.8 nm
Background
Aged Volcanic
Fresh Volcanic
Altitude (km)
35
30
25
20
15
10
0
20
40
60
80
100
Uncertainty of O_3 density (%)

Fig. 6

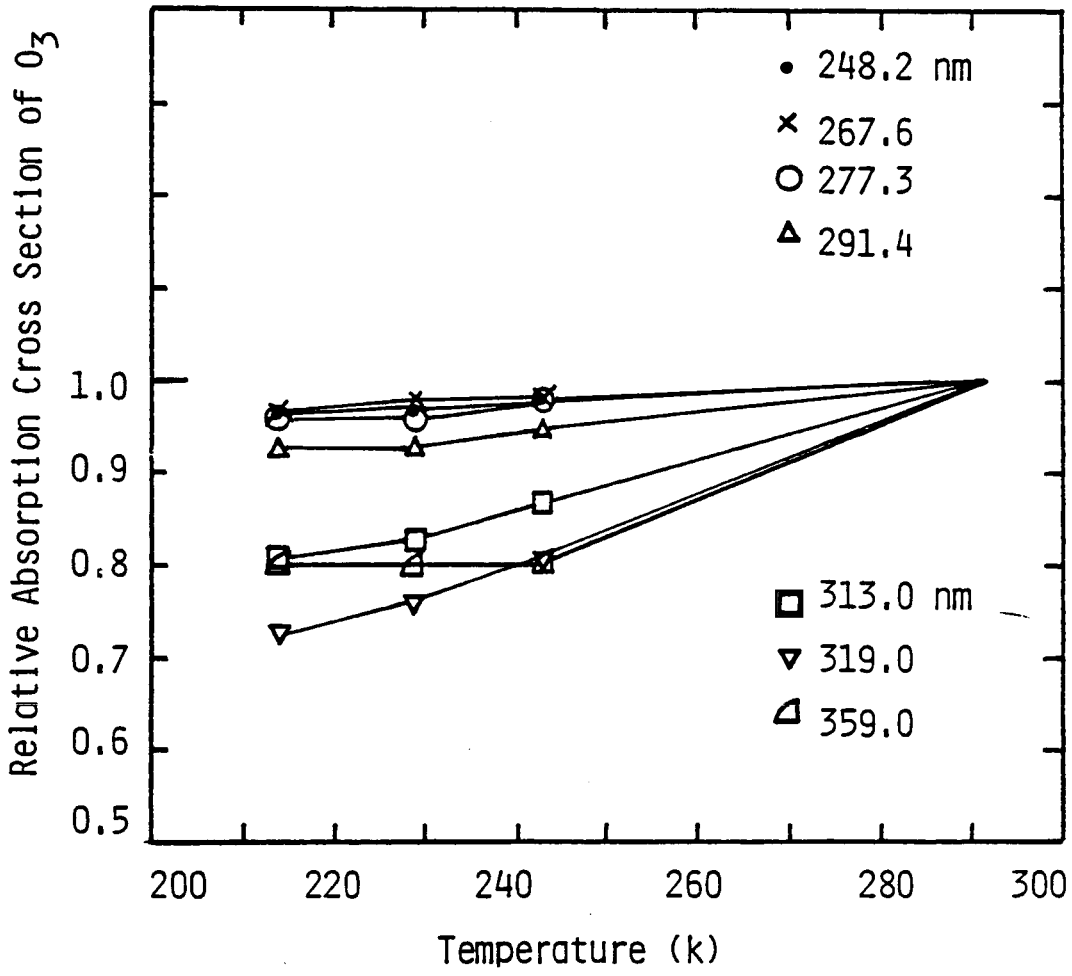
Relative Absorption Cross Section of O_3
1.0
0.9
0.8
0.7
0.6
0.5
200
220
240
260
280
300
Temperature (k)
248.2 nm
267.6
277.3
291.4
313.0 nm
319.0
359.0

Fig. 7

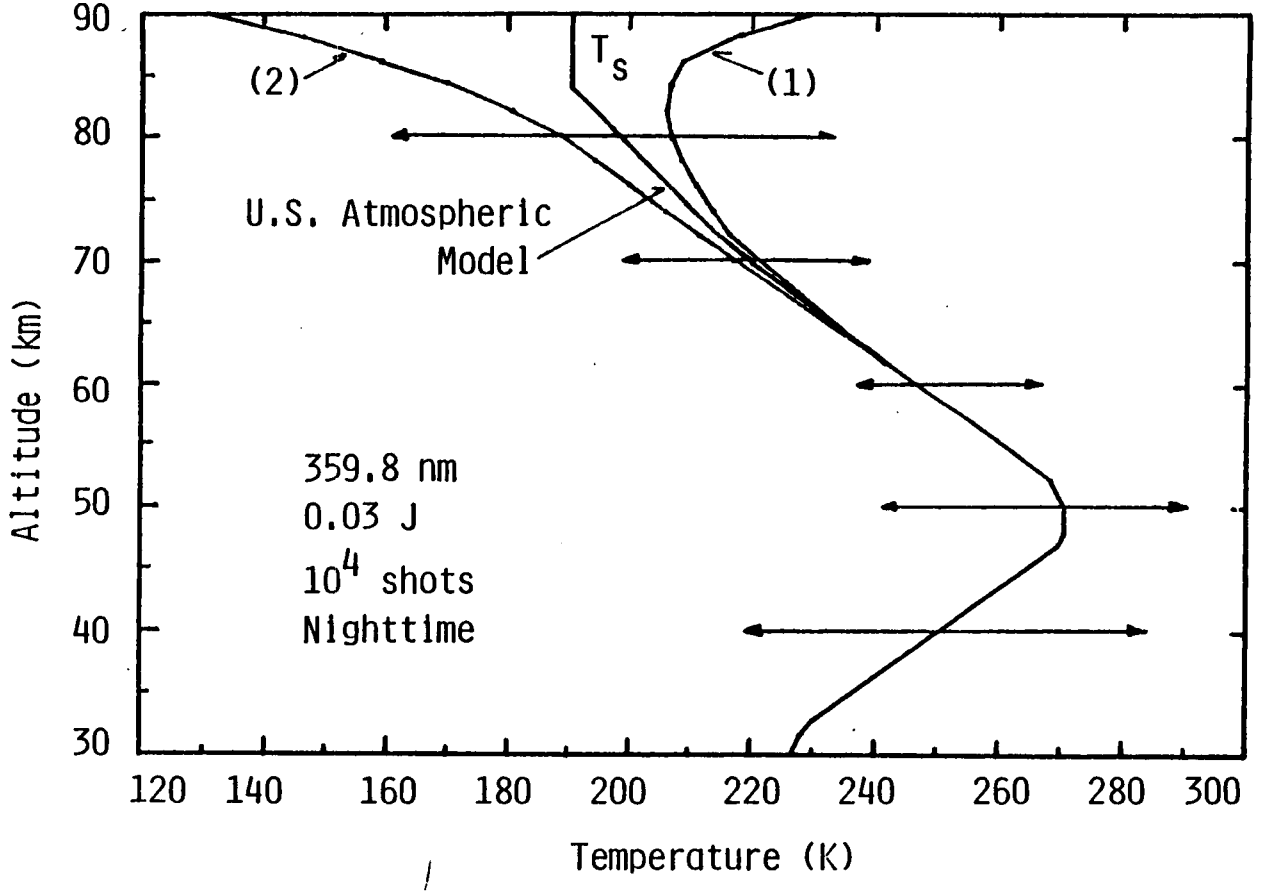
90
80
70
60
50
40
30
Altitude (km)
120
140
160
180
200
220
240
260
280
300
Temperature (K)
T_s
(1)
(2)
U.S. Atmospheric
Model
359.8 nm
0.03 J
10^4 shots
Nighttime

Fig. 8

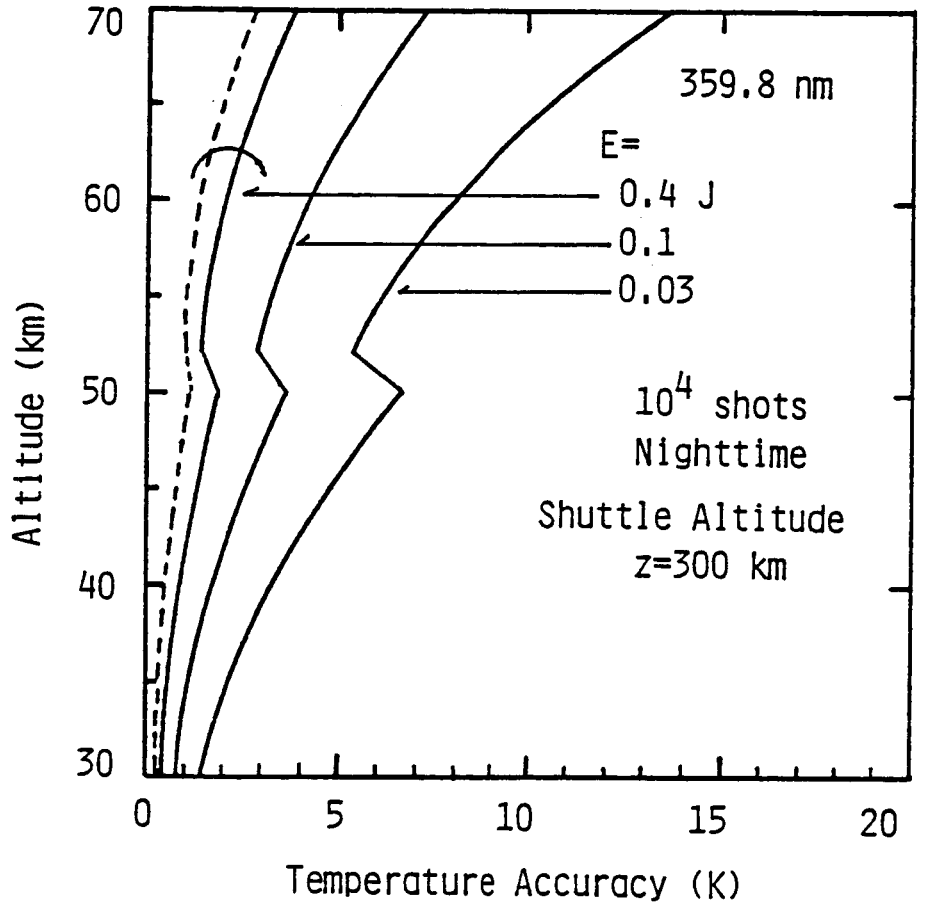
70
60
50
40
30
Altitude (km)
0
5
10
15
20
Temperature Accuracy (K)
359.8 nm
E=
0.4 J
0.1
0.03
10^4 shots
Nighttime
Shuttle Altitude
z=300 km

Fig. 9

ATMOSPHERIC OZONE MEASUREMENTS BY EXCIMER LIDARS

O. Uchino*, M. Maeda°, and T. Shibata°

*NASA Langley Research Center, Mail Stop 475
Hampton, VA 23666, USA
°Department of Electrical Engineering, Kyushu University,
Hakozaki, Fukuoka 812, Japan

Using an XeCl lidar, the first measurement of the vertical distribution of the stratospheric ozone was made at Fukuoka (33°N, 130°E) in July 1978 (Uchino et al., 1978). The method is a one-wavelength-absorption lidar with supporting meteorological data. Atmospheric molecular densities were obtained with daily meteorological radiosondes. The effect of the stratospheric aerosols on the measured ozone concentrations was corrected using data of scattering ratios observed by a ruby lidar. The method was promising for the continuous monitoring of the stratospheric ozone concentration (Uchino et al., 1979).

With a more compact and reliable XeCl laser, continuous ozone monitoring has been made at Fukuoka since September 1979 (Uchino et al., 1980). About fifty data sets were obtained. Figure 1 shows a typical data of the ozone concentrations. At around 20-25 km the measured errors are about 10 percent. Above this height range, the errors increase owing to decrease of the signal. At an altitude of 15 km they increase up to 10-20 percent due to decrease of the ozone concentrations and the effect of the aerosols.

Figure 2 shows the correlation between ozone mass mixing ratio measured by the XeCl lidar and temperature obtained by radiosondes at Fukuoka Meteorological Agency. The ozone mixing ratio has a high correlation with the temperature. This result is in good agreement with those obtained by ozonesondes at Tateno (36.1°N, 140.1°E) (Uchino et al., 1983a).

The effect of the stratospheric aerosol layer on the ozone concentrations was calculated from the scattering ratio data obtained by a frequency doubled Nd:YAG lidar, and estimated to be 10-20 percent in an altitude range of 15-20 km during 1979-1981 (Uchino et al., 1980). After the violent volcanic eruptions of Mt. El Chichon in early April 1982, the concentrations of the aerosols increased by a factor of 100 compared with those in the background level. For these many and variable aerosols, we developed a high power XeCl laser pumping a dye cell of p-terphenyl producing two wavelengths of 340.5 nm and 308 nm simultaneously.

Figure 3 shows the scattering ratio profiles at 340.5 nm calculated by an iterative method. A parameter of A is a ratio of extinction coefficient to backscattering coefficient of the aerosols. The maximum scattering ratio differs from about 18 percent at an altitude of 25 km for three values of A (Uchino, et al., 1984). A value of 22.7 was used for a bimodal size distribution measured by an optical counter in October 1982 and assuming 75 percent sulfuric acid particles. The backscattering coefficient and extinction coefficient at 308 nm were estimated from these data using Mie theory.

*Visiting Senior Research Scientist from Meteorological Research Institute, Tsukuba, Ibaraki 305, Japan

Figure 4 shows the ozone concentrations measured by this method. The fluctuation of the data is large in an altitude range of 23- 26 km. It might be the inhomogeneous aerosols (Pelon and Megie, 1982; Browell et al., 1985) and an uncertainty of the optical model of the aerosols. For increased stratospheric aerosols, a lidar with a wavelength pair of 308 nm and 313 nm is appropriate as shown later.

As the ozone concentrations decrease in the troposphere, shorter wavelengths are required. A high power KrF laser was developed for pumping a cell of methane gas. Emission of the second Stokes line (290.4 nm) of Stimulated Raman scattering (SRS) from methane and a XeCl laser (308 nm) was used for two-wavelength sources (Uchino et al., 1983b).

The ozone concentrations measured by this DIAL system are shown in Fig. 5. The Rayleigh component of the optical thickness was calculated from atmospheric molecular densities obtained by a radiosonde at Fukuoka Meteorological Agency. The differences of the backscattering coefficients and the Mie component of the optical thickness for the two wavelengths were neglected. The errors due to these neglects were estimated to be 1-2 percent above 4 km for a typical aerosol model. For more accurate estimation of errors due to the aerosols, an aerosol measurement at a third wavelength is available.

In the DIAL system, the output energy of 290.4 nm was relatively low (2-4mJ). To obtain more efficient SRS, we further developed a high power KrF laser with an automatic uv preionization (Shibata et al., 1985). The output power was increased by a factor of two compared with the former KrF laser, and the energy conversion efficiencies of the Stokes lines of hydrogen gas and methane gas were improved as shown in Fig. 6.

In Table 1 performances of current lidar system are shown. The maximum output energy per pulse of these SRS and excimer lasers are also shown. Figure 7 shows the ozone profile observed on December 7, 1984. The wavelengths used to observe each altitude range are also shown. The measurement error are within 30 percent except 13 - 18 km.

As conclusions, an XeCl lidar with supporting meteorological data is useful for the stratospheric ozone measurement for the background aerosols. In the upper stratosphere, a wavelength pair of XeCl and SRS of methane or hydrogen gas is promising (Werner et al., 1983).

For increased stratospheric aerosols, a lidar with a wavelength pair of 308 nm and 313 nm is applicable although the vertical resolution is two times lower than that of an XeCl lidar.

For the tropospheric ozone measurements, excimer lasers and SRS pumped by excimer lasers are useful. These lidar systems are comparatively simple configurations and they have possibilities of a high average power and a high repetition rate.

REFERENCES

Browell, E. V.; Ismail, S.; and Shipley, S. T., 1985: Ultraviolet DIAL Measurements of O_3 Profiles in Regions of Spatially Inhomogeneous Aerosols. Appl. Opt., vol. 24, no. 17, Sept. 1, pp. 2827-2836.

Hofmann, D. J.; and Rosen, M., 1983: Sulfuric Acid Formation and Growth in the Stratosphere Following the Eruption of El Chichon. Science, vol. 222, Oct. 21, no. 4621, pp. 325-327.

Pelon, J.; and Megie, G., 1982: Ozone Monitoring in the Troposphere and Lower Stratosphere: Evaluation and Operation of a Groundbased Lidar Station. J. Geophy. Res., vol. 87, no. C7, June 20, pp. 4947-4955.

Shibata, T.; Seki, K.; Hayami, T.; Kobuchi, M.; and Maeda, M., 1985: Observation of Atmospheric Ozone by a Differential Absorption Lidar Using Excimer Raman Lasers (in Japanese), Rev. Laser Eng., vol. 13, no. 3, March, pp. 60-68.

Uchino, O.; Maeda, M.; Kohno, J.; Shibata, T.; Nagasawa, C.; and Hirono, M., 1978: Observation of Stratospheric Ozone Layer by a XeCl Laser Radar. Appl. Phys. Lett., vol. 33, no. 9, Nov. 1, pp. 807-809.

Uchino, O.; Maeda, M.; and Hirono, M., 1979: Applications of Excimer Lasers to Laser-Radar Observations of the Upper Atmosphere. IEEE J. Quant. Electron., vol. QE-15, no. 10, Oct., pp. 1094-1107.

Uchino, O.; Maeda, M.; Shibata, T.; Hirono, M.; and Fujiwara, M., 1980: Measurement of Stratospheric Vertical Ozone Distribution with a XeCl Lidar; Estimated Influence of Aerosols. Appl. Opt., vol. 19, no. 24, Dec. 15, pp. 4175-4181.

Uchino, O.; Maeda, M.; Yamamura, H.; and Hirono, M., 1983a: Observations of Stratospheric Vertical Ozone Distribution by a XeCl Lidar. J. Geophys. Res., vo. 88, no. C9, June 20, pp. 5273-5280.

Uchino, O.; Tokunaga, M.; Maeda, M.; and Miyazoe, Y., 1983b: Differential-Absorption-Lidar Measurement of Tropospheric Ozone with Excimer-Raman Hybrid Lidar. Opt. Lett., vol. 8, no. 7, July, pp. 347-349.

Uchino, O.; Maeda, M.; Tokunaga, M.; Seki, K.; and Hayami, T., 1984: UV Lidar Measurement of Stratospheric Aerosol Layer; Observational Results at Fukuoka (33.6°N) During October 1982 through May 1983. J. Meteor. Soc. Japan, vol. 61, no. 2, April, pp. 357-362.

Werner, J.; Rothe, K. W.; and Walther, H., 1983: Monitoring of the Stratospheric Ozone Layer by Laser Radar. Appl. Phys., vol. B32, no. 3, Nov., pp. 113-118.

Table 1. Characteristics of Lidar System

Transmitter

Laser	KrF	KrF-pumped $H_2(S_1)$	KrF-pumped $CH_4(S_2)$	XeCl	KrF-pumped $H_2(S_2)$	XeCl-pumped p-Terphenyl
Wavelength (nm)	248.4	277.0	290.4	308.0	313.0	340.5
Absorption cross section (cm^2)	1.1×10^{-17}	5.0×10^{-18}	1.3×10^{-18}	1.3×10^{-19}	5.8×10^{-20}	1.5×10^{-21}
Maximum output energy per pulse (mJ)	508*	50	17	200	44	20
Pulse duration	15	10	10	15	10	10

*with stable resonator maximum pulse repetition rate 16 Hz

Receiver

Telescope	50 cm diameter (f=5255 cm) coude type
Field of view	1 mrad
Photomultiplier	EMI9558QB (2 ch.)
Filter bandwidth (transmission)	2 nm (10 %)
Seperation from laser system	3 m
Photon counter	
vertical resolution	1 μsec (δz=150 m)
channel number	1000
memory	floppy disk

FIGURE CAPTIONS

Fig. 1 Ozone concentrations and their standard deviations measured by an XeCl lidar.

Fig. 2 Correlation between ozone mass mixing ratio measured by an XeCl lidar and temperature obtained by radiosondes at Fukuoka Meteorological Agency.

Fig. 3 Vertical profiles of scattering ratio at a wavelength of 340.5 nm for three values of A.

Fig. 4 Ozone concentrations measured by two wavelengths of 308 nm and 340.5 nm.

Fig. 5 Ozone concentrations and their standard deviations measured by two wavelengths of 290.4 nm and 308 nm.

Fig. 6 Energy conversion efficiencies of H_2 and CH_4.

Fig. 7 Ozone concentration measured by lidar system in Table 1.

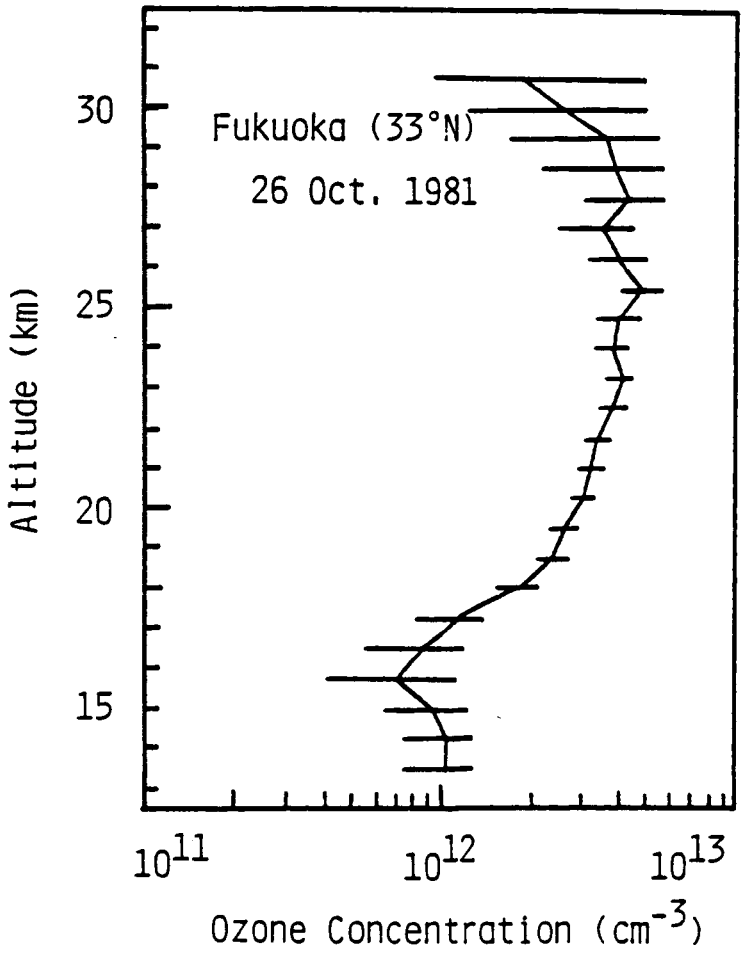
Fukuoka (33°N)
26 Oct. 1981
30
25
20
15
Altitude (km)
10^{11}
10^{12}
10^{13}
Ozone Concentration (cm^{-3})

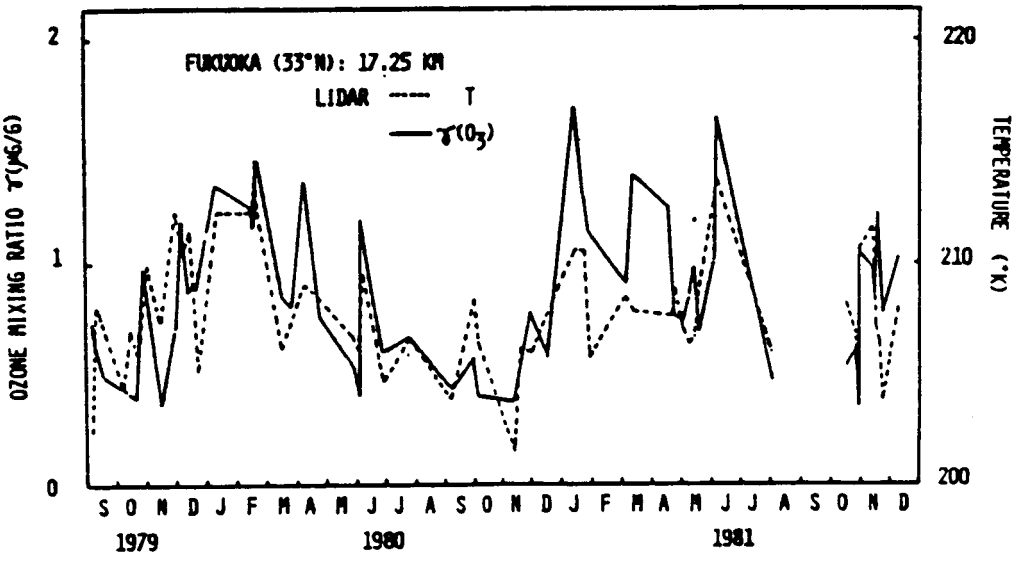
FUKUOKA (33°N): 17.25 KM
LIDAR ---- T
—γ(O3)
OZONE MIXING RATIO γ(μg/g)
TEMPERATURE (K)
2
1
0
220
210
200
S O N D J F M A M J J A S O N D J F M A M J J A S O N D
1979
1980
1981

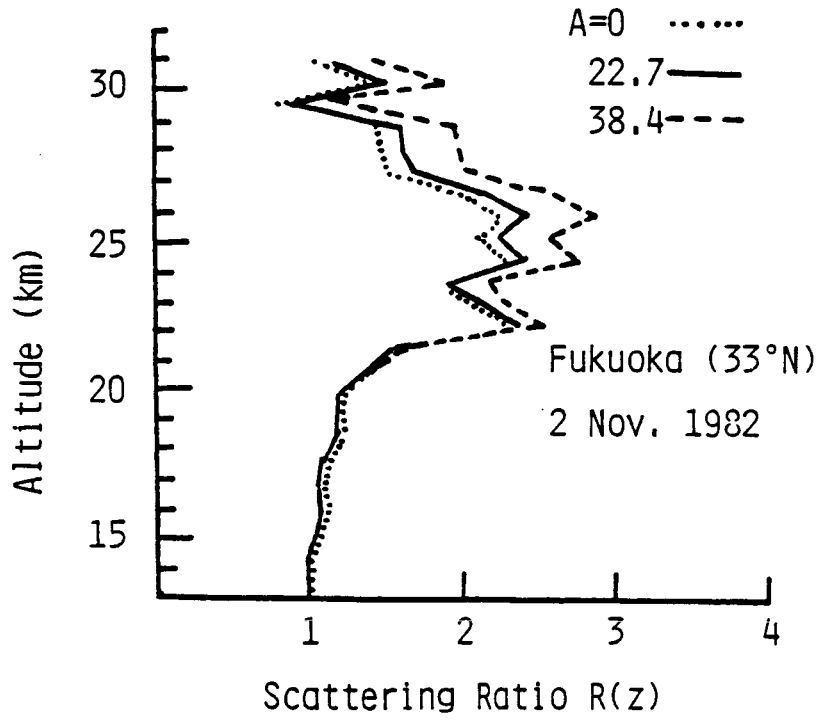
A=0
22.7
38.4
Fukuoka (33°N)
2 Nov. 1982
Altitude (km)
30
25
20
15
1
2
3
4
Scattering Ratio R(z)

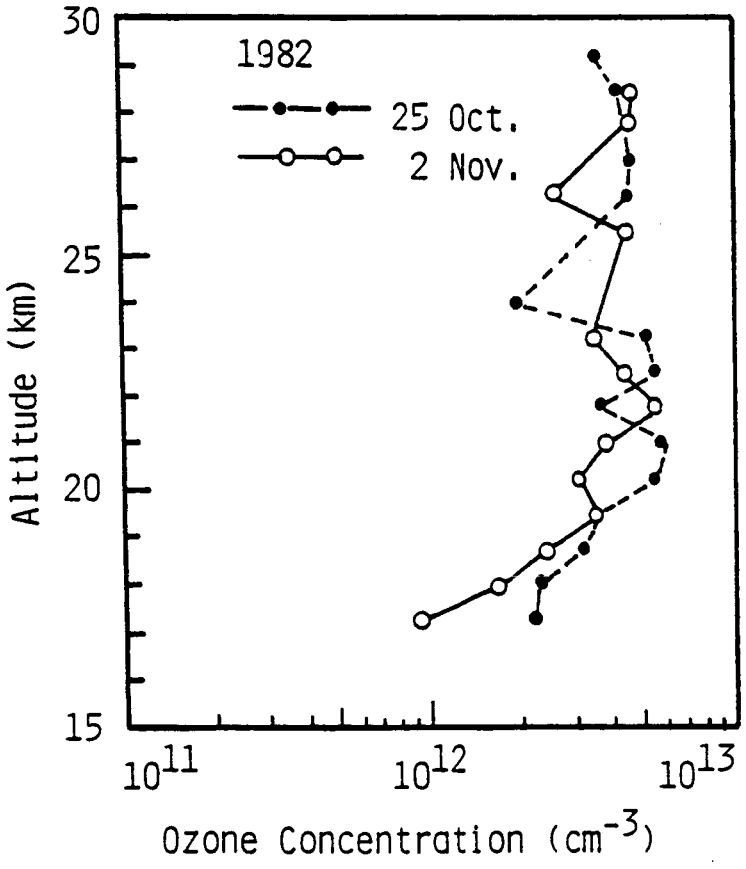
30
25
20
15
1982
25 Oct.
2 Nov.
Altitude (km)
10^{11}
10^{12}
10^{13}
Ozone Concentration (cm^{-3})

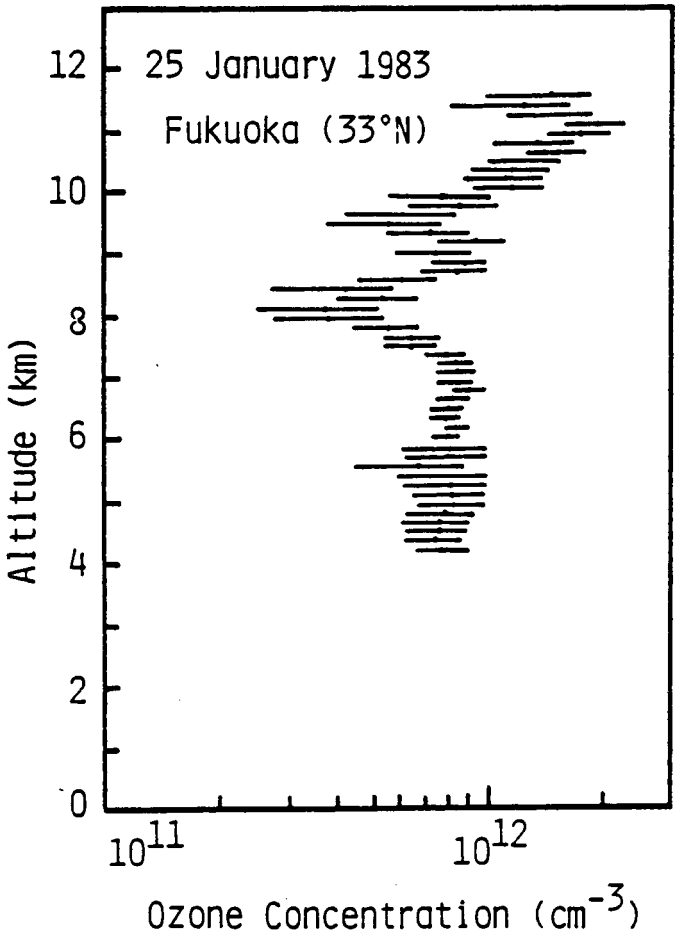
25 January 1983
Fukuoka (33°N)
Altitude (km)
12
10
8
6
4
2
0
10^{11}
10^{12}
Ozone Concentration (cm^{-3})

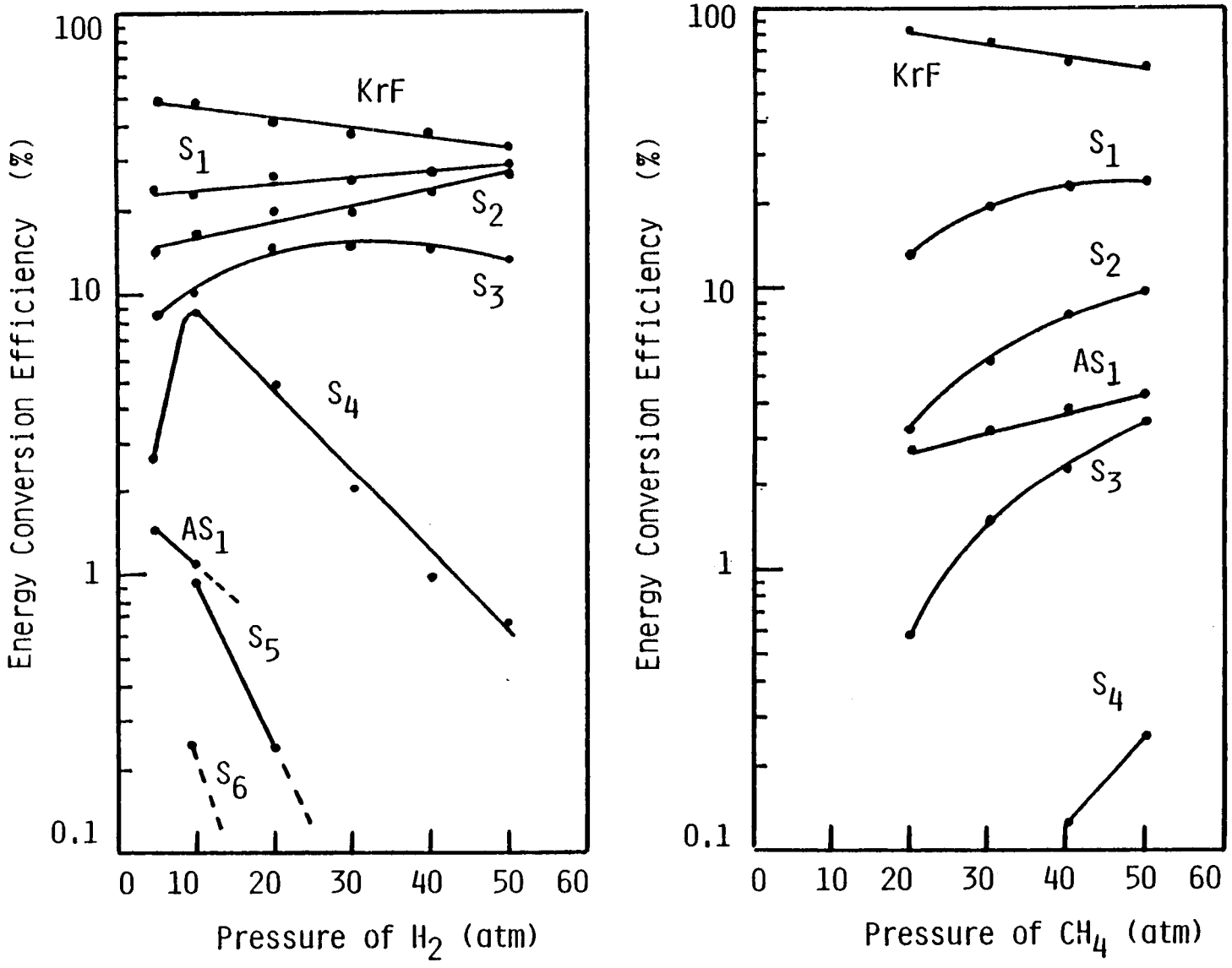
100
10
1
0.1
Energy Conversion Efficiency (%)
KrF
S1
S2
S3
S4
AS1
S5
S6
0 10 20 30 40 50 60
Pressure of H2 (atm)
100
10
1
0.1
Energy Conversion Efficiency (%)
KrF
S1
S2
AS1
S3
S4
0 10 20 30 40 50 60
Pressure of CH4 (atm)

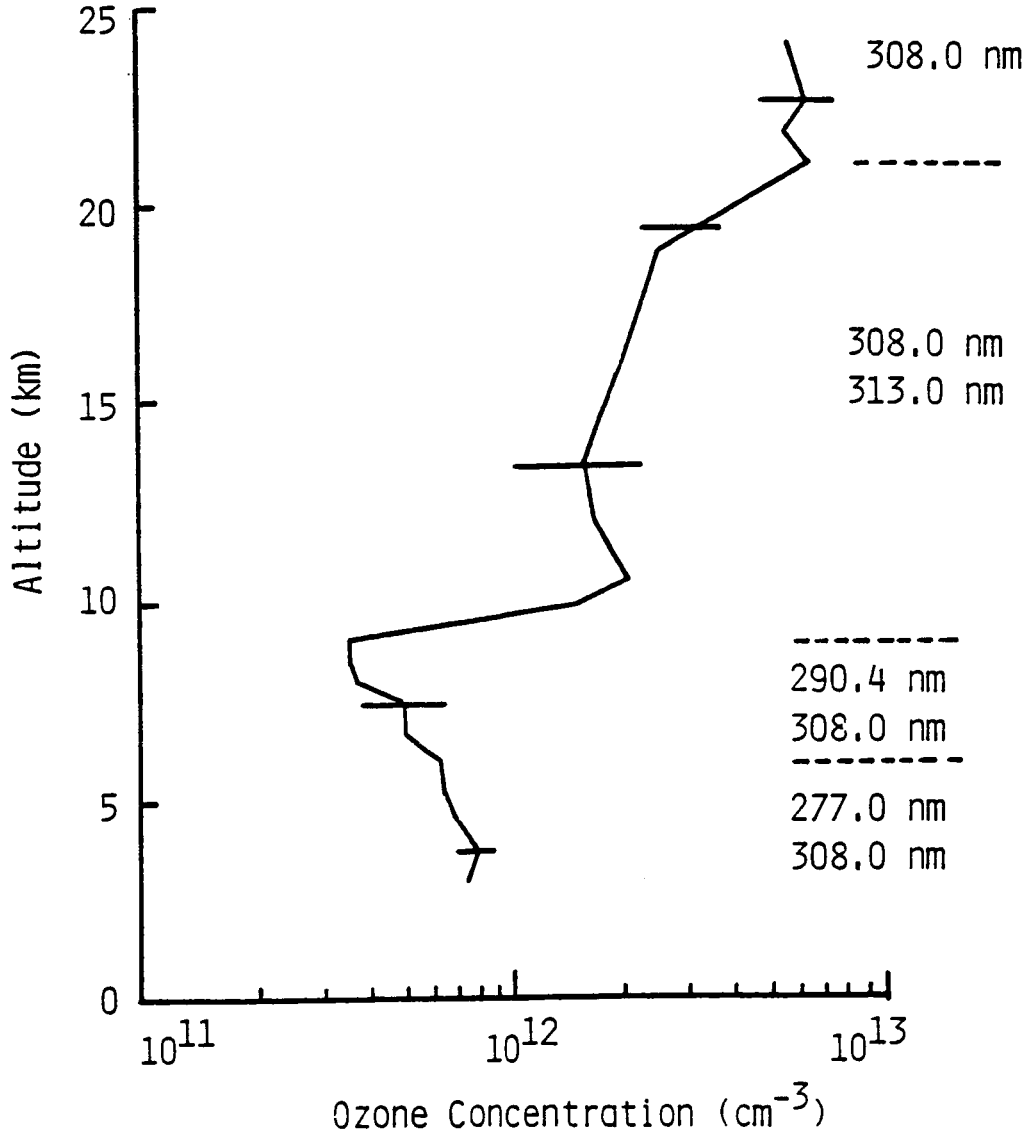
25
20
15
10
5
0
Altitude (km)
308.0 nm
308.0 nm
313.0 nm
290.4 nm
308.0 nm
277.0 nm
308.0 nm
10^{11}
10^{12}
10^{13}
Ozone Concentration (cm^{-3})